

A Morphological Study of Poly[bis(trifluoroethoxy)phosphazene] Using High Resolution Solid-State ^1H , ^{19}F , ^{31}P and ^{13}C NMR Spectroscopy

Alexey S. Borisov · Paul Hazendonk ·
Paul G. Hayes

Received: 28 September 2007 / Accepted: 6 October 2007 / Published online: 30 November 2007
© Springer Science+Business Media, LLC 2007

Abstract High-resolution ^{19}F , ^1H , ^{31}P and ^{13}C solid-state NMR methods were assessed to ascertain their suitability for studying the morphological behavior in the crystalline domain of phosphazene polymers with partially fluorinated side-chains. Poly[bis(trifluoroethoxy)phosphazene] (PBFP) was used as a sample system. Fast magic angle spinning (MAS), along with simultaneous ^{19}F and ^1H decoupling using the *xy*-16 sequence, were employed, as this has proven to greatly improve resolution in ^{13}C spectra of perfluorinated materials. Information obtained from Discrimination Induced by Variable Amplitude Minipulses (DIVAM) nutation experiments and cross-polarization (CP) methods aided the deconvolution analysis used to identify all components in the ^1H , ^{19}F and ^{13}C signals. DIVAM nutation experiments were also used to discriminate between signals from the amorphous and crystalline domain. The crystallinity in the solvent-cast PBFP was determined to be approximately 70%, which was seen to increase to approximately 80% in the heat-treated material, for all nuclei studied. A preliminary assignment was made for the crystalline signals in the ^1H and ^{13}C spectra to the α -, β - and γ -phases. Therefore, high-resolution ^{13}C and ^1H methods are valuable tools for morphological investigations into this class of polymer.

Keywords Poly[bis(trifluoroethoxy)phosphazene] · NMR · Solid state · MAS · DIVAM · Phosphazenes · Domain selection

1 Introduction

1.1 Overview

Inorganic–organic hybrid materials, such as polyphosphazenes, lie at the interference between organic, inorganic, and materials chemistry, are garnering increasingly more attention due to their potential applications. Currently, the most commonly utilized protocols for polyphosphazene preparation include both the age-old thermal ring-opening polymerization of hexachlorocyclotriphosphazene ($\text{N}=\text{PCl}_2$)₃ [1–4] and the cationic living polymerization of monomeric $\text{Me}_3\text{SiN}=\text{PCl}_3$ [5–7]. The resultant moisture sensitive polymer has received widespread attention, as evidenced by the synthesis of more than 600 derivatives which can be prepared via straightforward halogen substitution [8]. Indeed, polyphosphazenes have found application in novel battery technologies, biodegradable plastics, fire retardant additives, and biocompatible materials for human tissue engineering [9–13].

Despite the renewed interest in, and realized applications for polyphosphazene derivatives, a great deal remains to be uncovered regarding the relationship between polymer morphology and characteristics of the final material. A better understanding of how different morphologies affect the desirable macroscopic properties of the polymer is likely to provide the requisite information necessary for fine tuning substituted polyphosphazenes to best suit the application of interest.

This contribution focuses on the morphology of poly[bis(trifluoroethoxy)phosphazene] (PBFP, Fig. 1) using solid-state NMR spectroscopy. This polymer contains ^{13}C , ^1H and ^{19}F nuclei in side chains, and ^{31}P in the polymer backbone; hence NMR is an ideal structural probe for this system, provided sufficient spectral resolution can be obtained.

A. S. Borisov · P. Hazendonk (✉) · P. G. Hayes
Department of Chemistry and Biochemistry,
University of Lethbridge, 4401 University Dr,
Lethbridge, AB, Canada T1K 3M4
e-mail: paul.hazendonk@uleth.ca

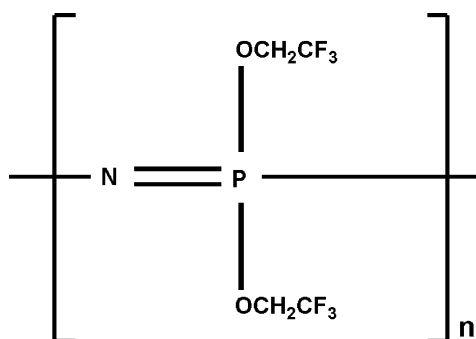
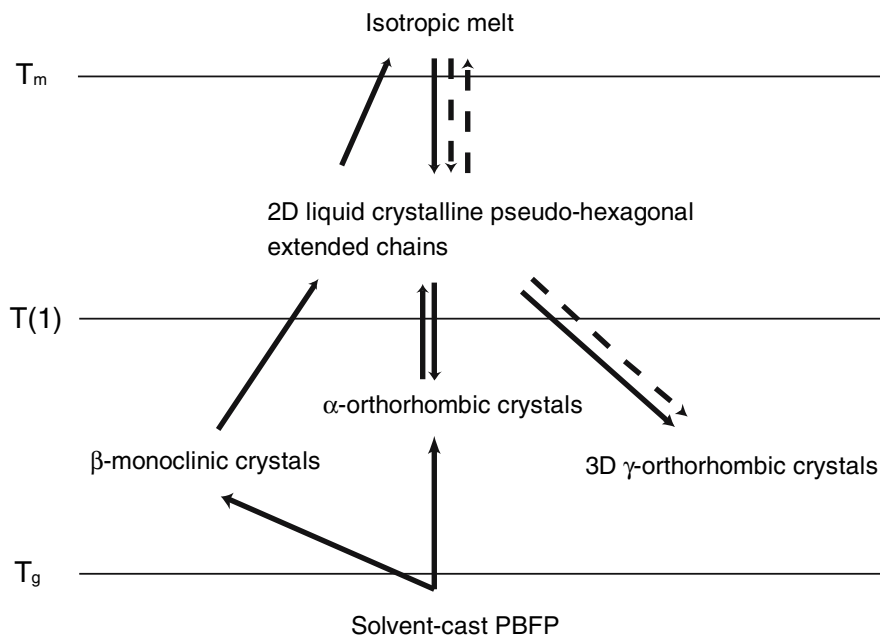


Fig. 1 Structure of the bis(trifluoroethoxy)phosphazene repeating unit

The morphological behavior in PBFP has been studied extensively by X-ray diffraction methods and differential scanning calorimetry (DSC) [14–16]. PBFP is an extremely hydrophobic semi-crystalline polymer, with transition temperatures that dramatically depend on its preparative methodology and thermal history. Specifically, melting points, T_m , vary between 218 °C and 250 °C; glass transitions, T_g , range from –82 °C to –62 °C, and its thermotropic transition, $T(1)$, occurs between 66 °C and 90 °C. [17] Studies by Allcock et al. [1] have demonstrated PBFP has five different phases: an amorphous phase, a liquid crystalline phase and three crystalline forms (Fig. 2). Powder X-ray diffraction studies report the unit cell dimensions of the α , β , and γ forms of the PBFP crystals while information pertaining to the kinetics of the transition from isotropic to mesophasic and from mesophasic to crystalline forms has been gleaned from DSC studies.

Fig. 2 Phase diagram indicating the morphological behaviour of PBFP



The PBFP samples utilized in these studies were generated from solvent-cast films and those requiring thermal history were obtained by heat cycling above $T(1)$. Samples which were cast at ambient temperature consist mainly of α -orthorhombic conformations with trace amounts of β -monoclinic crystals. Upon heating above $T(1)$ the polymer exists as 2D pseudo-hexagonal liquid crystals with extended chains, which then returns to the 3D α -orthorhombic state when cooled below $T(1)$, forming a 3D γ -orthorhombic extended chain system.

Heating of polymer samples repeatedly above $T(1)$, but below the melting point, T_m , tends to increase the $T(1)$ value and overall crystallinity. Heating above the melting point of the polymer, T_m , induces a reversible isotropic melt; the polymer returns to the 2D hexagonal structure when temperatures fall below T_m , and subsequently to the 3D γ -orthorhombic form below $T(1)$. It has been clearly shown that when materials are heat-treated for several cycles above T_m they are transformed permanently to the γ -orthorhombic conformation and do not return to the thermodynamically less favored 3D α -orthorhombic state [18, 19].

The above-described methods suffer from a plethora of disadvantages that prevents them from obtaining accurate structural details. Powder X-ray diffraction does not provide specific molecular information, only data on the unit cell. Furthermore, it cannot easily be used to study dynamic processes. Although DSC provides useful kinetic data on phase transitions, it lacks the ability to afford information at the molecular level. In contrast, solid-state NMR does not suffer from these limitations; therefore, both morphological changes and structural information can be obtained, provided certain experimental hurdles can be overcome.

1.2 Previous Studies of PBFP Using Solid-State NMR

Solid-state Nuclear Magnetic Resonance (SSNMR) methods were previously used to study the morphological behavior of PBFP [20]; however, the investigations were hampered by resolution so poor that no specific structural conclusions could be drawn regarding crystalline domain. Studies of PBFP using ^1H , ^{19}F and ^{31}P solid-state NMR spectroscopy consistently exhibited two signals corresponding to the crystalline and amorphous domains; however, these signals were largely broad featureless bands covering several kHz. When these samples were heated above the thermotropic transition temperature, they coalesced into a single, much narrower line corresponding to the mesophase structure. Recently, simultaneous ^1H and ^{19}F decoupling of polyphosphazene samples has made it possible to observe ^{13}C resonances [21]. These spectra demonstrated promise in giving structural details on the crystalline domain as some fine features could be discerned from both the CF_3 and CH_2 signals. Upon comparing subtle differences between heat-treated and solvent-cast films, these features were attributed to the two main crystalline forms. Again, the resolution was too poor to formulate assignments of these signals with any degree of confidence; however, it was claimed that if the resolution of ^{13}C NMR could be improved it should be possible to positively identify these signals.

1.3 Background on Solid-State NMR

NMR measurements in solids are primarily performed on powders, which are composed of small crystallites that are randomly oriented with respect to the magnetic field [22]. The resulting spectrum appears as a broad envelope, defined by the distribution in frequencies experienced by each crystallite, and is referred to as the powder pattern. When considering several nuclei in different chemical environments, the resulting spectrum, being the superposition of several powder patterns, becomes broad and featureless, often covering several kHz. It is not possible to extract useful structural information from a solid-state NMR spectrum in this form, except when considering only one isolated nucleus [22].

The solid-state NMR signal can be dramatically narrowed by spinning at the Magic Angle, 54.7° , with respect to the magnetic field. This removes the orientational dependence of the signal, effectively isotropically averaging it, as in solution [23, 24]. In order to achieve optimal averaging the spinning speed has to exceed the strength of all NMR interactions in the solid, which is often not possible. In such a situation the spectrum is composed of a series of side bands centered about the isotropic frequency and spaced by the spinning speed. Besides tremendous

improvements in resolution, an additional advantage to using Magic Angle Spinning (MAS) is that the signal is now dispersed about a series of sharp lines, rather than one broad featureless band, which results in a dramatic increase in the signal to noise ratio.

The hydrogen nucleus is 100% abundant, with a large magnetic dipole moment, resulting in very strong signals. Conversely, the dipolar couplings between protons are too strong to be effectively averaged by MAS, making high resolution elusive. In contrast, rare nuclei with small magnetic moments, such as carbon, nitrogen, and various transition metals, have weak NMR signals which are dispersed in frequency. Their signals can be enhanced by a technique known as cross-polarization, whereby the strong magnetization from nearby hydrogen nuclei is transferred to the weak nucleus [25–27]. In order to attain high resolution, high power ^1H decoupling [28] is required. In combination CP and MAS is the most commonly used experiment in SSNMR of weak nuclei [29].

1.3.1 High-Resolution ^{13}C NMR Spectroscopy in Fluoropolymers

When fluorine, also an abundant nucleus, is present in combination with hydrogen, simultaneous high power decoupling is required on both nuclei in order to observe carbon resonances. This is experimentally challenging as hydrogen and fluorine have frequencies that are very near one another, making it difficult to prevent their corresponding radio frequency channels from interfering with each other, especially at high powers. Recent modifications to probe circuit design, along with new high efficiency filters, have made it possible to achieve high power operation, 1 kW, with minimal interference. This ultimately allows for 30 dB isolation between the two channels [30]. With this advance an entirely new world is open to the spectroscopist whereby it is possible to study materials containing both nuclei. As a result, studies on partially fluorinated materials, such as organic and inorganic polymers, ceramics and glasses, modified biopolymers, and composite materials, are becoming much more common [31–34].

The addition of yet a third abundant nucleus, such as ^{31}P , complicates matters slightly. The ^{31}P frequency is far removed from ^1H and ^{19}F , therefore, a third isolated channel does not pose a serious technological challenge. Unfortunately, since one is generally interested in studying weak nuclei in the presence of these strong nuclei, a highly specialized four-channel probe is required which generally has to be custom made.

Although simultaneous decoupling of ^1H and ^{19}F from carbon is possible, obtaining sufficient spectral resolution

to discern sensitivity to differences in local structure has met with very little success [35]. At best, resolution of several kHz has been obtained for partially fluorinated materials. The difficulty with decoupling methods is that the decoupling efficiency is very strongly dependent on the frequency at which it is performed. When a large range of frequencies needs to be simultaneously covered, for example, the nucleus being decoupled has a large chemical shielding anisotropy, not all of the nuclei can be effectively decoupled at the same time. For ^1H , highly sophisticated phase-modulated multiple-pulse sequences have been developed for this purpose [36–39]; however, these sequences do not work well for ^{19}F as it tends to have very large chemical shielding anisotropies. Therefore, most decoupling is done with high power broadband irradiation, or simple multiple-pulse methods, accepting the low resolution as unavoidable.

Unfortunately most studies on polymeric systems need resolution better than a few hundred hertz. Recently Schmidt-Rohr et al. have demonstrated that when spinning samples above 20 kHz and using a sequence composed of a series of rotor synchronized 180° pulses, which follow a simple phase cycle, known as *xy-16*, very high resolution can be obtained for carbon in perfluorinated systems (~ 0.1 ppm (ca. 15–30 Hz for most spectrometers)) [40]. This improvement in resolution was attributed to a decrease in the frequency dependence of decoupling efficiency due to fast spinning, but also the removal of the one-bond ^{19}F – ^{13}C scalar couplings, which are typically on the order of a few hundred hertz. Therefore, the next logical step in studying partially fluorinated systems is to use *xy-16* decoupling on both ^1H and ^{19}F simultaneously, while concurrently spinning faster than 20 kHz.

One of the main roles of solid-state NMR in the study of materials is to characterize their domain structure. Therefore, a way to select a signal from a single structural domain is desired. This can be achieved in a myriad of ways by exploiting the relaxation and spin-dynamics properties typical of the abundant nuclei [41, 42]. Usually separate experiments are required to select for the amorphous and crystalline domains. The amorphous domains tend to be mobile and disordered, hence their chemical shielding and dipolar coupling interactions are reduced by motion. As a consequence, they tend to have longer relaxation times, smaller chemical shielding anisotropies and weaker dipolar couplings than the crystalline domain which is generally ordered and rigid. As such, amorphous signals characteristically have narrow lines while resonances from crystalline domains tend to be broad.

Recently a new domain selective experiment was proposed that can be tuned to select for either amorphous or crystalline domains. The Discrimination Induced by Variable Angle Minipulse (DIVAM) sequence [20, 42–44], can

separate signals on the basis of either relaxation or spin-dynamics properties. It is composed of twelve low-amplitude pulses followed by a 90° observation pulse. For small minipulse angles selection is achieved through relaxation differences, while at larger angles, selection is based on differences in the size of the chemical shielding anisotropy. Narrow amorphous components nutate with the minipulse angle, while the crystalline signal lags behind, and sometimes, never truly nutates. Each component of the signal will therefore invert (cross-zero) at different minipulse angles. In this manner one can determine the number of components that compose the signal and whether they exhibit amorphous or crystalline behavior.

1.4 Objectives

We propose to use fast MAS, ca. 25 kHz, in combination with *xy-16* simultaneous ^{19}F and ^1H decoupling, to obtain high resolution ^{19}F , ^1H , ^{31}P and ^{13}C spectra for preparations of PBFP known to have different morphological compositions. It is anticipated that the improved resolution will reveal fine structure in the NMR signal, which ultimately can be related to the morphology of the polymer. The DIVAM sequence will be used to determine and identify the components within the signal. This investigation is therefore a test to see whether current state-of-the-art high-resolution methods for $^1\text{H}/^{19}\text{F}$ solid-state NMR are suited to study morphological behavior in phosphazene polymers.

2 Experimental

2.1 General Procedures

All NMR spectra were obtained using a Varian INOVA 500 spectrometer operating at 499.84 MHz for ^1H , 125.68 MHz for ^{13}C , 470.332 MHz for ^{19}F and 202.34 MHz ^{31}P , equipped with a 4-channel HFX MAS NMR probe with a 2.5 mm outer rotor diameter. All experiments were carried out at a MAS rate of 25 kHz. The ^{19}F NMR spectra were referenced to external CFCl_3 by setting this signal to 0 ppm, the ^1H and ^{31}P spectra were referenced externally to TMS by setting its signal to 0 ppm. ^{13}C spectra were referenced externally to adamantane setting the CH_2 peak to 38.6 ppm. The high-resolution ^{13}C NMR spectroscopy was performed using $\{^1\text{H}, ^{19}\text{F}\}$ *xy-16* decoupling. Pulse lengths for ^1H , ^{19}F , ^{31}P and ^{13}C direct polarization experiments were set to 3.5, 3.25, 4.25 and 4 respectively with relaxation delays of 5, 5, 10, and 5 s, respectively. In the ^1H to ^{13}C and ^{19}F to ^{13}C CP experiments the contact times were set to 2 ms for both

samples. The ^1H and ^{19}F DIVAM nutation experiments were carried out over 50 minipulses in 1.83° increments. Unless otherwise noted, all chemicals were purchased from Sigma-Aldrich and used as received.

2.2 High-temperature Synthesis via the Ring-opening Polymerization of Hexachlorocyclotriphosphazene

Hexachlorocyclotriphosphazene (2.00 g, 17.2 mmol) was loaded into a Pyrex polymerization tube in an MBraun glove box. The tube was then evacuated for 30 min, flame sealed and placed in an oven at 250°C . The polymerization tube was constantly agitated throughout the process (20 h or until the contents became viscous) by placement within a receptacle kept in continuous motion via attachment to a variable speed electrical motor. The resultant rubbery poly(dichlorophosphazene) was a translucent, colorless solid and is highly soluble in polar organic solvents such as THF. The polymer is highly air sensitive, undergoing rapid hydrolysis of P–Cl bonds upon exposure to trace moisture. The corresponding P–O–P crosslinked polymers are largely insoluble in common solvents, and thus, undesirable for subsequent modifications. In order to circumvent such crosslinking, samples of poly(dichlorophosphazene) were converted to the well-known derivative, poly[bis(trifluoroethoxy)-phosphazene] via reaction with sodium trifluoroethoxide (*vide infra*).

2.3 Preparation of Sodium Trifluoroethoxide

Sodium trifluoroethoxide was prepared by adding fresh Na metal (5.75 g, 0.250 mol) to a 250 mL two-neck round bottomed flask charged with THF (75 mL) and equipped with a stir bar and condenser. The reaction was carried out under a dry argon atmosphere. Subsequently 2,2,2-trifluoroethanol (15.0 mL, 0.210 mol) was added dropwise via syringe to the above-mentioned mixture. The solution was heated to reflux and allowed to stir for 4 h, after which it was cooled to room temperature and allowed to stir for an additional 12 h to ensure complete reaction. The mixture was filtered through a medium porosity sintered glass funnel and subsequently cannula transferred to a 150 mL bomb for future use.

2.4 Preparation of Poly[bis(trifluoroethoxy)phosphazene]

The unsubstituted polymer was extracted from the polymerization tube using benzene (3×15 mL) and transferred to a 250 mL round bottomed flask containing

100 mL of benzene. The reaction mixture was then added dropwise to a rapidly stirring THF solution of sodium trifluoroethoxide (6.1 mL, 17 mmol). The mixture was heated to reflux for 3 h and allowed to cool to room temperature for an additional 12 h under an atmosphere of dry argon. The solvent was removed under reduced pressure and the solids were washed with water (3×30 mL) to remove occluded sodium chloride. The substituted polymer was dissolved in THF (5 mL) and precipitated via dropwise addition to rapidly stirring hexane (100 mL). The polymer was further separated from excess sodium trifluoroethoxide and low molecular weight products by repeating this process twice more with acetone (5 mL) as the solvent. The resultant white fibrous material was dried under vacuum (16 h) before further use.

2.5 Polymer Sample Preparation

Solvent-cast PBFP was prepared by dissolving 0.5 g of polymer in 3 mL of acetone and pouring the solution onto a glass plate. The solvent was allowed to evaporate under ambient conditions. The polymer film was then scraped off the glass plate and loaded into a 2.5 mm rotor.

2.6 Preparation of Heat-treated Samples

The heat-treated material was obtained by heating the polymer over 11 cycles. During each cycle the sample was repeatedly annealed for a minimum of one hour at 120°C prior to cooling to 22°C .

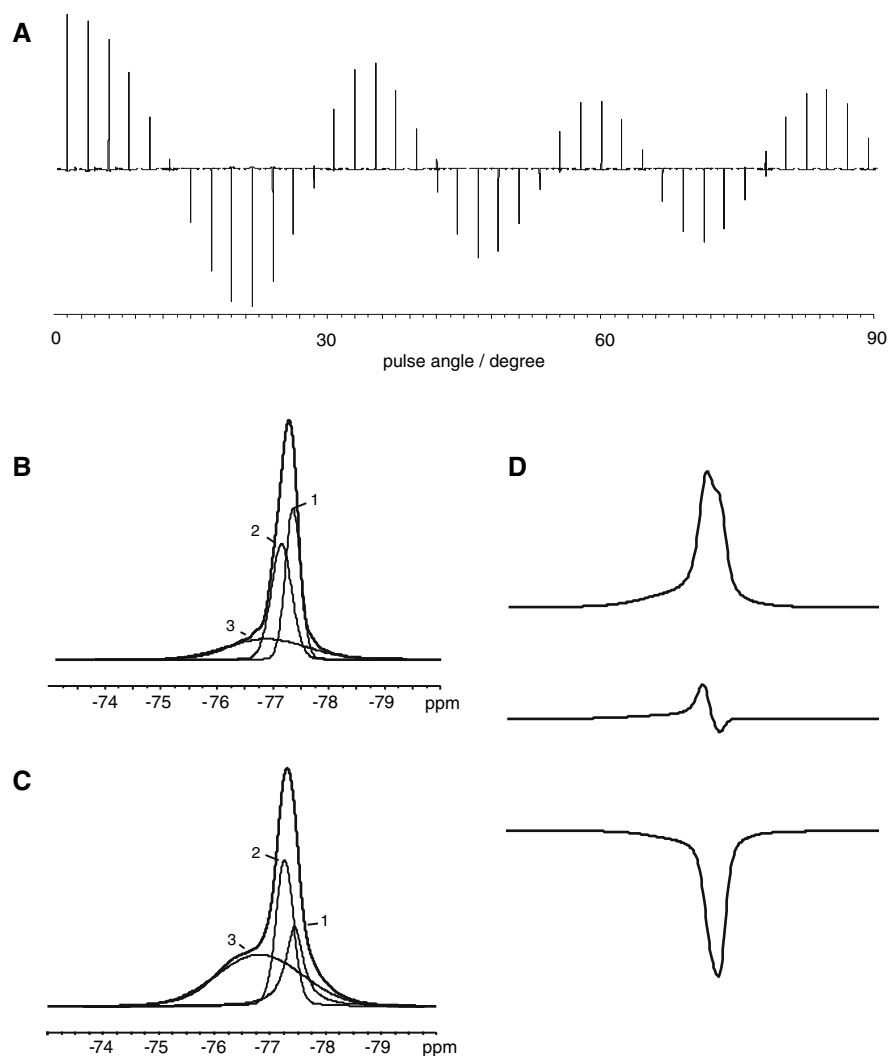
3 Results and Discussion

3.1 ^{19}F Solid-state MAS NMR of PBFP

The ^{19}F solid-state NMR spectra of the solvent-cast and heat-treated PBFP are shown in Fig. 3b and 3c, respectively. Each spectrum features one signal at -77.6 ppm, which upon a closer inspection appears to be made up of two overlapping lines. The narrow, intense component is assumed to correspond to the highly mobile disordered amorphous phase of the polymer, and the broad component corresponds to its rigid ordered crystalline phases. This assignment was made on the basis of the behavior of the linewidth with temperature where the amorphous signal is seen to broaden dramatically upon cooling.

The ^{19}F Direct-DIVAM nutation experiment is shown for the solvent-cast polymer, in Fig. 3a. The spectra near the first zero-crossing, at a minipulse angle of 12.6° (Fig. 3d) show that three separate lines cross zero at

Fig. 3 (a) Room temperature ^{19}F direct DIVAM nutation experiment of the solvent-cast PBFP, spinning at 25 kHz. (b) Room temperature deconvolved ^{19}F solid-state NMR spectrum of the solvent-cast pbfp spinning at 25 kHz. (c) Room temperature deconvolved ^{19}F solid-state NMR spectrum of the heat-treated PBFP spinning at 25 kHz. (d) The ^{19}F direct DIVAM spectra for minipulse angles near the first zero-crossing point at 9, 10.8 and 12.6° respectively (top to bottom)



slightly different minipulse angles. This suggests that there are three contributions to the spectrum, one broad and two narrow lines, where the nutation rate of one of the narrow lines, peak 2, and the broad line, peak 3, are similar.

These spectra were subjected to deconvolution analyses, where it was determined that the narrow part of the signal is composed of two lines with widths of 31 and 42 Hz for the solvent-cast material, and 32 and 39 Hz for the heat-treated PBFP, respectively. The broad component is composed of a single peak, 176 Hz wide at -76.8 ppm. If one were to assume that the narrow components correspond to the amorphous domain, and the broad component to the crystalline domain, the deconvolution data (Table 1), suggest, when comparing solvent-cast and heat-treated PBFP side by side, that the overall contribution from the amorphous phase changes from 70.6% to 51.6% of total peak area, respectively. This supports the notion that the heat cycling increases the overall crystallinity. This assignment forces one to conclude that this method suffers from

limited spectral resolution and therefore cannot offer detailed information on the crystalline morphology.

An alternative interpretation would assign one of the narrow peaks, 2, to the crystalline domain, based on its DIVAM nutation behavior, leaving only one peak, 1, which is also the narrowest, belonging to the amorphous domain. In this case, the crystallinity is 70.4% in the solvent-cast polymer, which changes to 78.1% upon heat treatment. Therefore, the crystalline domain has two peaks assigned to it, 2 and 3. Since 3 increases and 2 decreases in intensity with heat treatment, 3 must contain γ -phase, 2 has α -phase, and the β -phase could be part of either peak.

3.2 ^1H Solid-state MAS NMR of PBFP

The ^1H solid-state MAS NMR spectra of PBFP are presented in Fig. 4b for the solvent-cast material and Fig. 4c for the heat-treated material. Each spectrum features one

Table 1 Results from the deconvolution analysis of the ^{19}F , ^1H and ^{31}P spectra of PBFP

Sample	Solvent-cast					Heat-treated				
	1	2	3	4	5	1	2	3	4	5
^{19}F										
Chemical shift (ppm)	-77.6	-77.2	-76.8			-77.6	-77.2	-76.8		
Width (Hz)	31	42	176			32	39	176		
Area (a.u.)	86 (34.6%)	89.9 (36%)	73.3 (29.4%)			53.8 (21.9%)	72.83 (29.7%)	119 (48.4%)		
^1H										
Chemical shift (ppm)	4.69	4.7	4.72	4.73	7.2	4.69	4.7	4.72	4.73	7.2
Width (Hz)	11.1	23.8	21.9	215	501	12.4	21.8	17.8	216	429
Area (a.u.)	7.3 (23.8%)	6.3 (20.4%)	8.8 (28.6%)	4.8 (28.6%)	3.6 (11.6%)	4.9 (18.5%)	3.7 (13.9%)	2.8 (10.5%)	11.9 (45%)	3.2 (12.1%)
^{31}P										
Chemical shift (ppm)	-3.5	-3.1	0.71			-3.5	-3.1	0.71		
Width (Hz)	123.2	149.5	341.4			123.2	149.5	363.1		
Area (a.u.)	15.4 (38.4%)	20.1 (50.3%)	4.5 (11.3%)			4.6 (15.1%)	17.6 (57.9%)	8.21 (27%)		

intense narrow peak at 4.6 ppm, which appears to be composed of several lines, and one very broad peak at 7.2 ppm. The spectra from the ^1H Direct-DIVAM nutation experiments for the solvent-cast material are seen in Fig. 4a. Near the first zero-crossing, around a minipulse angle of 12.6° (Fig. 4d), for the signal at 4.6 ppm, three narrow components are observed to cross zero at slightly different angles before the broad component crosses. In this case two of the narrow components nutate similarly to the broad component.

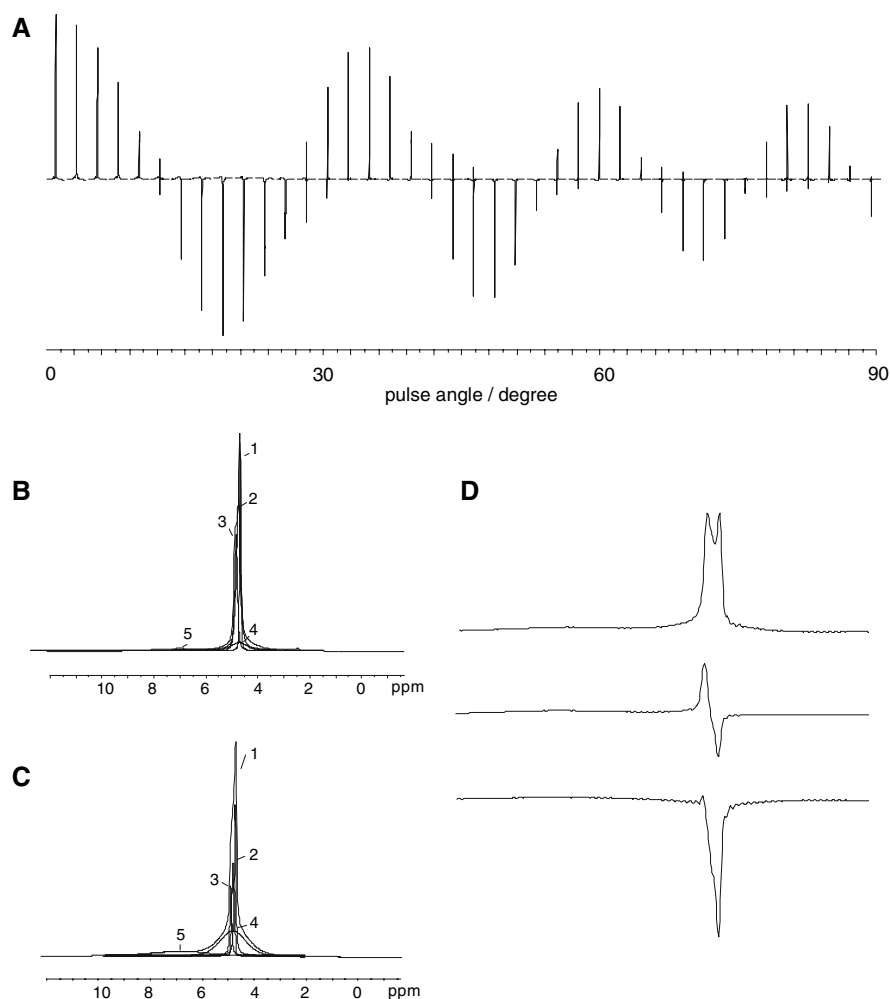
The signal at 4.6 ppm was deconvolved into four components, three of which are narrow, and are assumed to correspond to the amorphous phase (mobile), whilst the fourth is broad, and together with a peak at 7.2 ppm, is assigned to a crystalline (rigid) phase. Upon closer inspection of the deconvolution results, shown in Table 1, it becomes apparent that the amorphous phase constitutes 72.8% of the total peak area of the solvent-cast material, while only 42.9% of the heat-treated material. These results are consistent with the first interpretation of the ^{19}F experiments. Again, this forces one to conclude that this method lacks sufficient resolution to elucidate more than two lines for the crystalline signal, and is thereby not able to contribute new information about its crystalline morphology.

An alternative assignment, based on the DIVAM nutation behavior observed of two of the narrow peaks, 2 and 3, would attribute them to the crystalline domain, leaving only one peak, 1, corresponding to the amorphous domain. In this case, the crystallinity is 76.2% in the solvent-cast material and 81.5% in the heat-treated polymer. Now, there are four lines assigned to the crystalline domain. Upon heating, peaks 2 and 3 decrease in similar proportion, peak 4 increases dramatically, and peak 5 remains unchanged. This is consistent with 2 and 3 corresponding to the α -phase, 4 to the γ -phase, and 5 to the β -phase.

3.3 ^{31}P Solid-state MAS NMR of PBFP

The ^{31}P NMR spectra (not shown) contain one narrow intense peak at -3.5 ppm and a small broad peak at 0.7 ppm. The deconvolution analysis suggests that the narrow peak is composed of two lines, 123 and 149 Hz wide, respectively. The results are given in Table 1. If the narrow signal is assumed to correspond to the amorphous phase and the broad signal to the crystalline phase, the overall amorphous contribution is 89.1% of the total peak area of the solvent-cast material, which decreases to 73.0% in the heat-treated polymer. Alternatively, only one narrow peak can be taken to represent the amorphous domain, peak 1, as it decreases dramatically in intensity upon heat treatment. In this case the crystallinity in the solvent-cast

Fig. 4 (a) Room temperature ^1H direct DIVAM nutation experiment of the solvent-cast PBFP, spinning at 25 kHz. (b) Room temperature deconvolved ^1H solid-state NMR spectrum of the solvent-cast PBFP, spinning at 25 kHz. (c) Room temperature deconvolved ^1H solid-state NMR spectrum of the heat-treated PBFP, spinning at 25 kHz. (d) The ^1H direct DIVAM spectra for minipulse angles near the first zero-crossing point at 9, 10.8 and 12.6° respectively (top to bottom)



material is 61.6%, which increases to 84.5% with heat cycling. The latter interpretation is consistent with the ^1H and ^{19}F results. Again, too few crystalline signals are apparent to draw any morphological conclusions.

3.4 ^{13}C Solid-state MAS NMR of PBFP

The direct-polarization ^{13}C spectrum, and the ^1H - ^{13}C and ^{19}F - ^{13}C CP MAS NMR spectra obtained using simultaneous ^1H and ^{19}F xy -16 decoupling of solvent-cast and heat-treated PBFP, are shown in Figs. 5, 6, and 7. These spectra contain two signals at 11 and 71 ppm respectively, corresponding to the CH_2 and CF_3 carbons. This assignment, initially made on the basis of chemical shifts, was confirmed by gating the ^1H and ^{19}F decoupling, where the corresponding carbon signal would split or broaden due to the heteronuclear coupling interactions being reintroduced [20]. Each peak exhibits fine structure, reflecting various contributions from different environments within the polymer. Due to instrument time restraints it was not

practical to use direct DIVAM nutation experiments on ^{13}C to determine the number of components in each signal. Instead, both DP and CP spectra were collected, where the relative intensities of each component vary between them, according to their CP efficiencies. Although in most cases the resolution was sufficient to identify all components, the additional CP spectra allowed independent confirmation of the number of components.

Figure 5a shows the ^{13}C solid-state NMR spectra of the solvent-cast and heat-treated PBFP, on the left- and right-hand sides, respectively. Figure 5b contains expansions of the spectral regions corresponding to the CF_3 carbon. The deconvolution analysis reveals 6 contributions to this signal. The carbon resonance of the CH_2 group is depicted in Fig. 5c and is found to consist of 5 components. The deconvolution results of both spectral regions of the solvent-cast and heat-treated polymer are summarized in Table 2.

The deconvolution analysis of the CF_3 and CH_2 regions for both materials were independently verified with separate analyses of the ^{19}F - ^{13}C CP (Fig. 6) and ^1H - ^{13}C CP

Fig. 5 ^{13}C DP solid-state NMR spectrum of PBFP Using $\{^1\text{H}, ^{19}\text{F}\}$ $xy-16$ decoupling, obtained at spinning rate of 25 kHz at room temperature. (a) Left: Solvent-cast PBFP. Right: Heat-treated PBFP. (b) Left: expansion of the CF_3 region of the solvent-cast PBFP. Right: expansion of the CF_3 region of the heat-treated PBFP. (c) Left: expansion of the CH_2 region of the solvent-cast PBFP. Right: expansion of the CH_2 region of the heat-treated PBFP

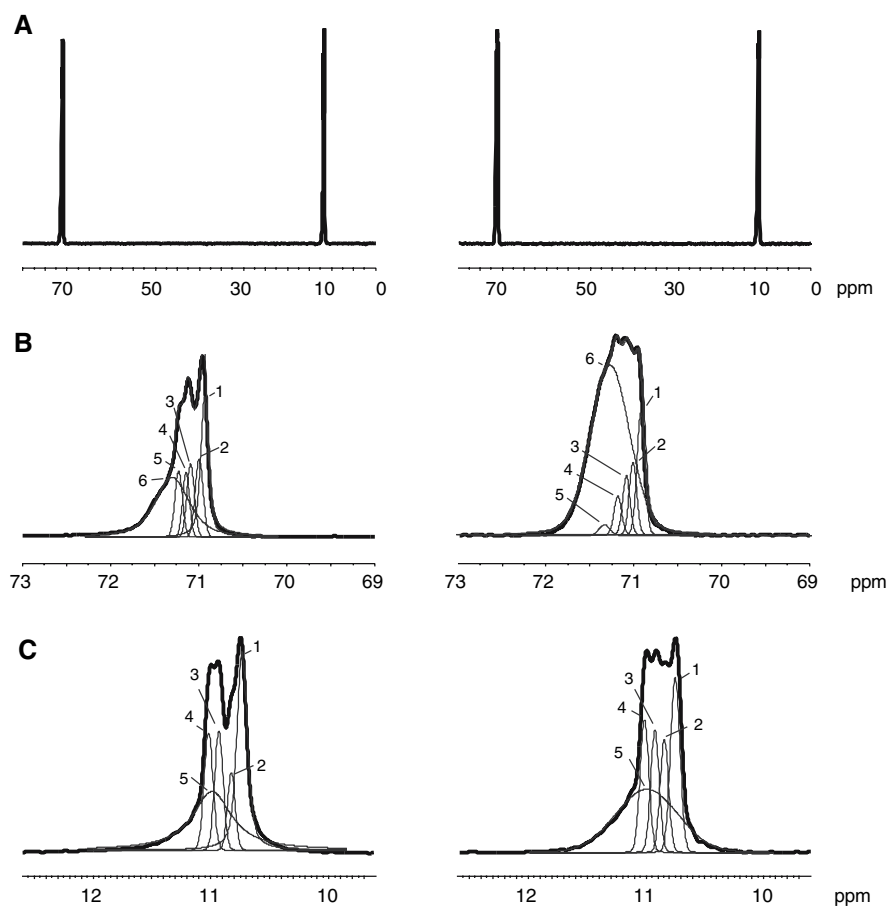
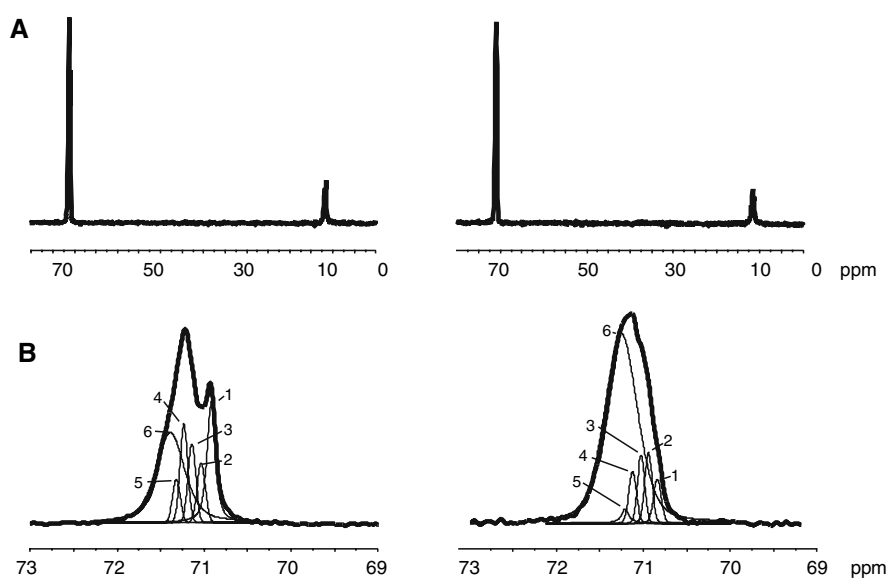


Fig. 6 $^{19}\text{F}-^{13}\text{C}$ CP solid-state NMR spectrum of PBFP using $\{^1\text{H}, ^{19}\text{F}\}$ $xy-16$ decoupling, obtained at spinning rate of 25 kHz at room temperature. (a) Left: Solvent-cast PBFP. Right: heat-treated PBFP. (b) Left: expansion of the CF_3 region of the solvent-cast PBFP. Right: expansion of the CF_3 region of the heat-treated PBFP



(Fig. 7) spectra, respectively. In each case a consistent model was attained preserving the number of components, the frequency, width, and Gaussian nature of the lines.

The six components in the CF_3 signal are divided amongst the amorphous and crystalline domains based on their CP behavior. When comparing the DP spectrum of the

solvent-cast polymer, in Fig. 5b, with the corresponding ^{19}F CP spectrum, in Fig. 6b, peak 1 is significantly attenuated, attributing it to the amorphous domain. This leaves the remaining peaks, 2–5, assigned to the crystalline domain, which all have significantly increased intensity in the CP spectra. Confirmation of this assignment is seen in

Fig. 7 ^1H - ^{13}C CP solid-state NMR spectrum of PBFP using $\{^1\text{H}, ^{19}\text{F}\}$ xy-16 decoupling, obtained at spinning rate of 25 kHz at room temperature. (a) Left: solvent-cast PBFP Right: heat-treated PBFP. (b) Left: expansion of the CH_2 region of the solvent-cast PBFP. Right: expansion of the CH_2 region of the heat-treated PBFP

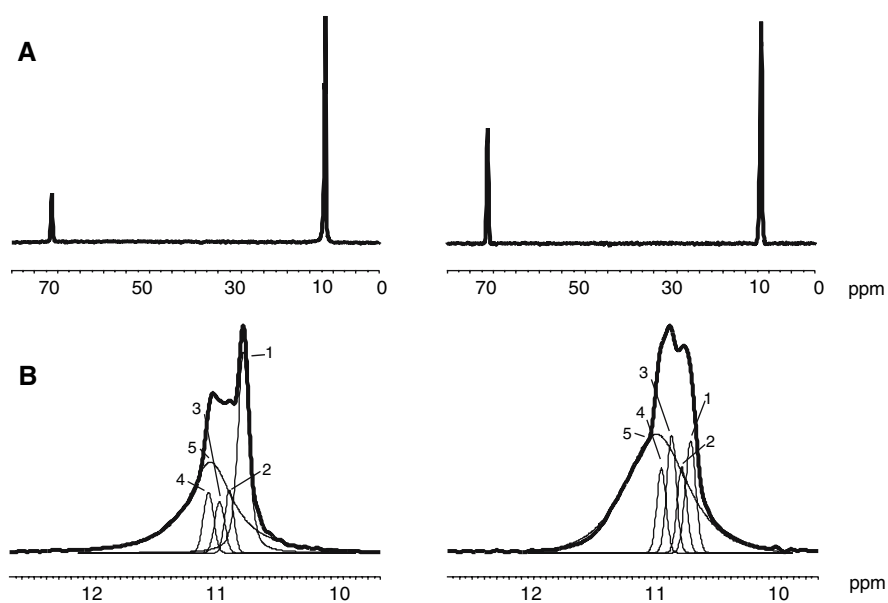


Table 2 Results from the deconvolution analysis of the ^{13}C spectra of PBFP

Sample	Solvent-cast						Heat-treated					
	1	2	3	4	5	6	1	2	3	4	5	6
CF_3												
Chemical shift (ppm)	70.89	71.04	71.38	71.26	71.58	71.75	70.91	71.13	71.31	71.55	71.69	71.79
Width (Hz)	30.5	30.5	26.8	29.2	28.9	113.7	31.8	30.1	30.7	30.1	28.9	135.4
Area DP (a.u.)	106.47	47.76	34.64	42.7	38.18	183.77	42.19	23.93	20.98	13.98	1.96	283.81
Area CP (a.u.)	14.47	5.31	6.63	8.3	3.59	37.13	2.3	3.54	3.29	2.65	0.98	46.83
% of Total DP signal	23.5	10.5	7.6	9.4	8.4	40.5	10.9	6.2	5.4	3.6	0.5	73.6
% of Crystalline DP signal		13.8	10	12.3	11	53		6.9	6.1	4.1	0.6	82.3
CH_2												
Chemical shift (ppm)	11.01	11.2	11.47	11.67	11.57		11.01	11.22	11.42	11.64	11.55	
Width (Hz)	30.7	22.5	24.8	26.1	116.8		29.1	26.1	26.4	27.6	195	
Area DP (a.u.)	137.79	32.12	53.95	56.12	165.88		49.85	28.85	31.47	35.65	133.67	
Area CP (a.u.)	52.53	10.73	9.87	11.84	104.07		11.13	7.73	10.78	7.42	89.15	
% of Total DP signal	30.9	7.2	12.1	12.6	37.2		17.8	10.3	11.3	12.8	47.8	
% of Crystalline DP signal		10.4	17.5	18.2	53.8			12.6	13.7	15.5	58.2	

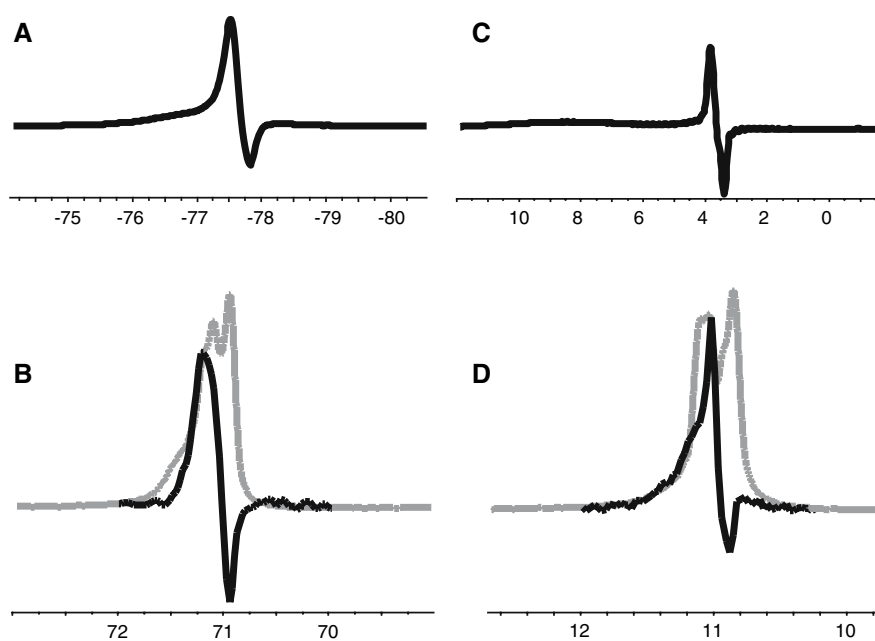
the ^{19}F - ^{13}C CP DIVAM spectrum (Fig. 8b), at a minipulse angle where the amorphous signal in the ^{19}F DIVAM nutation spectrum is inverted (Fig. 8a), and peak 1 is found to be correspondingly inverted. Similarly, the CH_2 region is decomposed into 5 lines, where again peak 1 is seen to be inverted in the ^1H - ^{13}C CP DIVAM spectrum (Fig. 8d) at a minipulse angle at which the amorphous signal in the ^1H DIVAM nutation spectrum is inverted (Fig. 8c).

According to the deconvolution results of the CH_2 region, the total crystalline component increases from 69.1 to 82.2%, upon heat treatment. The CF_3 signal indicates the same trend whereby the crystallinity increases

from 76.4 to 89.1%. These results are consistent with those observed for ^1H , ^{19}F and ^{31}P , in which the solvent-cast material is predominantly crystalline, and the crystallinity increases upon heat treatment.

Changes observed in the distribution of the crystalline domain signals (Table 2) between the solvent-cast and heat-treated material facilitate the assignments of the crystal phases. For the CH_2 signal, peaks 3 and 4 decrease, 5 increases, and 2 increases moderately. This is consistent with peaks 3 and 4 being assigned to the α -phase, peak 5 to the γ -phase and peak 2 to the β -phase. The CF_3 signal has 6 peaks, of which only peak 6 can be assigned with any

Fig. 8 ^{19}F and ^1H CP DIVAM spectra of the solvent-cast material for the CF_3 (b) and CH_2 (d), signals. The DP signals are shown in the background for comparison. The ^{19}F (a) and ^1H (c) DIVAM nutation spectra are shown above, at a minipulse angle near the first zero-crossing



confidence to the γ -phase, as it is the largest, and increases with heat cycling. All the remaining peaks decrease, meaning that any one of them could correspond to the α -phase, and at this stage it is not clear which corresponds to the β -phase.

4 Conclusions

- High resolution was achieved in the ^1H , ^{19}F , and ^{31}P NMR spectra of PBFPP using fast Magic Angle spinning. Most significantly, fine structure was observed in the ^1H spectrum, owing to linewidths ranging from 10 to 500 Hz, which is unusually narrow and probably due, in part, to high mobility in the polymer.
 - High resolution ^{13}C NMR spectra were obtained using a combination of fast Magic Angle Spinning and simultaneous ^{19}F and ^1H decoupling with the xy -16 sequence. Fine structure in the ^{13}C signals of both the CF_3 and CH_2 , was found to be consistent with that observed in the ^1H , ^{19}F and ^{31}P spectra.
 - For all nuclei studied the crystallinity in the PBFPP samples was seen to increase from approximately 70% to 80% upon heat cycling.
 - Using information obtained from CP and DIVAM nutation experiments all signals in the ^{19}F , ^1H , and ^{13}C experiments were decomposed into their constituent lines using deconvolution analysis.
 - Using information from the CP and DIVAM nutation experiments the lines in each spectrum were assigned to the crystalline and amorphous domains.
- In the ^1H and ^{13}C spectra sufficient signals were found to belong to the crystalline domain to make preliminary assignments to the α , β and γ -phase.
 - More domain-selective high-resolution NMR studies will be required to independently verify these assignments.

Acknowledgements We thank the Natural Sciences and Engineering Research Council of Canada, the Canadian Foundation for Innovation, the Alberta Network for Proteomics Innovation and the University of Lethbridge for financial support. We also wish to thank Dr. C. deDenus, Hobart and William Smith Colleges, Geneva, New York, and Dr. A. R. McWilliams, Ryerson University, Toronto, Ontario, for their invaluable advice. We would like to acknowledge Dr. Dinu Iuga for his help in setting up the experiments and in the operation of the spectrometer.

References

- H.R. Allcock, *J. Inorg. Organomet. P. Mat.* **16**, 277 (2007)
- H.R. Allcock, *Chemistry and Application of Polyphosphazenes* (Wiley & Sons, New York, 2003)
- J.E. Mark, H.R. Allcock, R. West, *Inorganic Polymers* (Prentice Hall, Englewood Cliffs, New York, 1992)
- R.H. Neilson, P. Wisian-Nielson, *Chem. Rev.* **88**, 541 (1988)
- C.H. Honeyman, I. Manners, C.T. Morrissey, H.R. Allcock, *J. Am. Chem. Soc.* **117**, 7035 (1995)
- H.R. Allcock, J.M. Nelson, C.R. de Denus, I. Manners, *Tailored Polymers and Applications* (VSP International Science Publishers, Netherlands, 2000), p. 165
- B. Wang, Rivard E., Manners I, *Inorg. Chem.* **41**, 1690 (2002)
- Allcock H.R., *Appl. Organometal. Chem.* **12**, 659 (1998)
- S.G. Kumbar, S. Bhattacharyya, S.P. Nukavarapu, Y.M. Khan, L.S. Nair, C.T. Laurencin, *J. Inorg. Organomet. P.* **16**, 4 (2006)
- J. Luten, J.H. van Steenis, R. van Someren, J. Kemmink, N.M.E. Schuurmans-Nieuwenbroek, G.A. Koning, D.J.A. Crommelin,

- C.F. van Nostrum, W.E. Hennink, J. Control Release. **89**, 483 (2003)
11. S. Lakshmi, D.S. Katti, C.T. Laurencin, Adv. Drug Deliv. Rev. **55**, 467 (2003)
12. H. Kawakami, S. Kanezaki, M. Sudo, M. Kanno, S. Nagaoka, S. Kubota, Artif. Organs. **26**, 10 (2002)
13. A.K. Andrianov, J. Inorg. Organomet. P. **16**, 4 (2006)
14. P. van Mourik, E. Veldman, B. Norder, J. van Turnhout, M. Wuebbenhorst, J. Mater. Sci. **40**, 1661 (2005)
15. R.J. Ciora, J.H. Magill, Macromolecules. **23**, 2350 (1990)
16. E. Corradi, A. Farina, M.C. Gallazzi, S. Bruckner, S.V. Meille, Polymer **40**, 4473 (1999)
17. N.S. Schneider, C.R. Desper, R.E. Singler, J. Appl. Polym. Sci. **20**, 3087 (1976)
18. M. Kojima, J.H. Magill, Makromol. Chem. **186**, 649 (1985)
19. M. Kojima, J.H. Magill, Polymer. **26**, 1971 (1985)
20. P. Hazendonk, C. de Denu, A. Iuga, P. Cahoon, B. Nilsson, D. Iuga, J. Inorg. Organomet. P. **16**, 4 (2006)
21. P. Holstein, U. Scheler, R.K. Harris, Magn. Reson. Chem. **35**, 647 (1997)
22. M.H. Levitt, *Spin Dynamics, Basics of Magnetic Resonance* (John Wiley & Sons, Ltd, Chichester, 2001)
23. E.R. Andrew, A. Bradbury, R.G. Eades, Nature **182**, 1659 (1958)
24. I.J. Lowe, Phys. Rev. Lett. **2**, 258 (1959)
25. A. Pines, M.G. Gibby, J.S. Waugh, J. Chem. Phys. **59**, 569 (1973)
26. S.R. Hartmann, E.L. Hahn, Phys. Rev. **128**, 2042 (1962)
27. A. Pines, M.G. Gibby, J.S. Waugh, J. Chem. Phys. **56**, 1776 (1972)
28. A.E. Bennet, C.M. Rienstra, M. Auger, K.V. Lakshmi, R.G. Griffin, J. Chem. Phys. **103**, 6951 (1995)
29. E.O. Stejskal, J. Schaefer, J.S. Waugh, J. Magn. Reson. **28**, 105 (1977)
30. C. Luchinat, M. Piccioli, R. Pierattelli, F. Engelke, T. Marquardsen, R. Ruin, J. Magn. Reson. **150**, 161 (2001)
31. R. Hill, A. Calver, S. Skinner, A. Stamboulis, R. Law, Key Eng. Mat. **309**, 305 (2006)
32. K.M. Miller, Prog. NMR Spectrosc. **28**, 255 (1996)
33. Harris R.K., P. Jackson, Chem. Rev. **91**, 1427 (1991)
34. S. Ando, R.K. Harris, U. Scheler, *Encyclopedia of NMR, Advances in NMR*, vol 9 (John Wiley and Sons, Ltd, Chichester, 2002), p. 531
35. G. De Paepe, B. Elena, L. Emsley, J. Chem. Phys. **121**, 3165 (2004)
36. G. De Paepe, P. Hodgkinson, L. Emsley, Chem. Phys. Lett. **376**, 259 (2003)
37. D. Sakellariou, A. Lasege, P. Hodgkinson, L. Emsley, Chem. Phys. Lett. **319**, 253 (2000)
38. M. Ernst, A. Samoson, B.H. Meier, J. Chem. Phys. **123**, 6 (2005)
39. S.-F. Liu, K. Schmidt-Rohr, Macromolecules. **34**, 8416 (2001)
40. R.K. Harris, G.A. Monti, P. Holstein, *Solid-state NMR of Polymers, Studies in Physical and Theoretical Chemistry*, vol. 84 (Elsevier Science B.V., 1998)
41. S. Ando, R.K. Harris, P. Hazendonk, P. Wormald, Macromol. Rapid Commun. **26**, 345 (2005)
42. P. Wormald, B. Ameduri, R.K. Harris, P. Hazendonk, Solid-state Nucl. Mag. **30**, 114 (2006)
43. P. Hazendonk, T. Montana, A. Iuga, P. Wormald, Mater. Res. Soc. **984** (2007)
44. P. Hazendonk, R.K. Harris, S. Ando, P. Avalle, J. Magn. Reson. **162**, 206 (2003)